Coherence Field Theory • Perturbation Theory

CFT Feynman Rules and Interaction Diagrams

Perturbative Series Decomposition of the Five Canonical Interactions

GPE action functional • Bogoliubov propagators • Contact and phonon-exchange vertices
IX1 vortex–antivortex annihilation • IX2 same-charge repulsion • IX3 soliton elastic collision
IX4 dark soliton × vortex • IX5 breathing mode × soliton impurity

Abstract. Every scattering or interaction process in Coherence Field Theory (CFT) admits a perturbative series expansion in powers of the nonlinear coupling g, organised by Feynman diagrams drawn from a small set of propagators and vertices derived from the Gross–Pitaevskii (GPE) action. This document derives those rules from first principles, catalogues the propagator and vertex factors, and works out the leading-order (and, where relevant, resummed exact) diagrammatic decomposition of the five canonical CFT interaction scenarios: vortex–antivortex annihilation (IX1), same-charge vortex repulsion (IX2), bright soliton head-on collision (IX3), dark soliton × vortex composite (IX4), and breathing-mode condensate perturbed by a soliton impurity (IX5). The CFT *coupling constant* $\alpha_{\mathrm{CFT}} = mg/\hbar^2$ is of order unity at the fixed-point scale ξ, making the theory strongly coupled. The exact results quoted throughout — Bogoliubov dispersion, vortex–vortex logarithmic potential, soliton phase shift, Kohn breathing frequency — correspond to resummations of the perturbative series to all orders; they are exact because the underlying system is integrable or admits an exact semiclassical solution.

Contents

1 The CFT Action Functional and Path Integral

1.1 Lagrangian density

The coherence field $\psi(\mathbf{r},t)\in\mathbb{C}$ is described by the action functional

$$S[\psi^*,\psi]=\int_0^T dt\int d^2r\,\mathcal{L},\qquad \mathcal{L}=i\hbar\psi^*\partial_t\psi-\frac{\hbar^2}{2m}|\nabla\psi|^2-V(\mathbf{r})|\psi|^2-\frac{g}{2}|\psi|^4. \tag{1}$$

The Euler–Lagrange equation $\delta S/\delta\psi^*=0$ recovers the Gross–Pitaevskii equation (GPE):

$$i\hbar\,\partial_t\psi=-\frac{\hbar^2}{2m}\nabla^2\psi+V(\mathbf{r})\psi+g|\psi|^2\psi. \tag{2}$$

The term $i\hbar\psi^*\partial_t\psi$ is the *Berry phase* (kinematic) term; it does not contribute to the energy but generates the Magnus force on topological defects (Section 4).

1.2 Global symmetries and conserved currents

Symmetry	Generator	Conserved charge
$U(1)$ global phase: $\psi\to e^{i\theta}\psi$	$Q=\int\lvert\psi\rvert^2\,d^2r$	Norm (particle number)
Spatial translation: $\mathbf{r}\to\mathbf{r}+\mathbf{a}$	$\mathbf{P}=\frac{\hbar}{2i}\int(\psi^*\nabla\psi-\text{c.c.})\,d^2r$	Momentum
Galilean boost	$\mathbf{K}=m\mathbf{P}\,t-m\mathbf{r}Q$	Centre-of-mass velocity
Topological $\mathbb{Z}$: winding	$n=\frac{1}{2\pi}\oint\nabla\arg\psi\cdot d\boldsymbol{\ell}$	Vortex charge (per core)

1.3 The path integral and perturbative expansion

The quantum partition function is

$$Z=\int\mathcal{D}\psi^*\,\mathcal{D}\psi\;\exp\!\Big(\tfrac{i}{\hbar}S[\psi^*,\psi]\Big). \tag{3}$$

Splitting $S=S_0+S_{\rm int}$ with

$$S_0=\int dt\,d^2r\Big[i\hbar\psi^*\partial_t\psi-\tfrac{\hbar^2}{2m}|\nabla\psi|^2-V|\psi|^2\Big], \tag{4}$$

$$S_{\rm int}=-\frac{g}{2}\int dt\,d^2r\;|\psi|^4, \tag{5}$$

and expanding $e^{iS_{\rm int}/\hbar}=\sum_{n=0}^{\infty}\frac{1}{n!}\big(iS_{\rm int}/\hbar\big)^n$, each term is evaluated by Wick's theorem using the free propagator G_0 derived from S_0. The result is the standard Feynman diagram expansion; at n-th order there are n interaction vertices and the diagrams are all possible Wick contractions of the $4n$ fields.

Strong coupling caveat. The dimensionless coupling is $\alpha_{\rm CFT}\equiv mg/\hbar^2$. In all CFT simulations we use dimensionless units $\hbar=m=1$ with $g=1$, giving $\alpha_{\rm CFT}=1$. The perturbative series in $\alpha_{\rm CFT}$ is therefore an asymptotic expansion, not a convergent one. The exact results obtained

for the Bogoliubov spectrum, the vortex logarithmic potential, and the soliton S-matrix are *non-perturbative resummations*; they hold exactly because the relevant subsystem is integrable (NLSE in 1D) or semiclassically exact.

2 Bogoliubov Decomposition and Quadratic Theory

2.1 Condensate background

Fix the uniform condensate background $\psi_0(\mathbf{r},t) = \sqrt{\rho_0}\, e^{-i\mu t/\hbar}$ with chemical potential $\mu = g\rho_0$. Write the full field as a fluctuation around this background:

$$\psi(\mathbf{r},t) = e^{-i\mu t/\hbar}\big(\sqrt{\rho_0} + \delta\psi(\mathbf{r},t)\big), \quad \delta\psi = u + iv \text{ (real amplitude and phase parts).} \tag{6}$$

Substituting into (2) and retaining terms up to second order in $\delta\psi$:

$$i\hbar\partial_t \begin{pmatrix} u \\ v \end{pmatrix} = \begin{pmatrix} 0 & \hat{h}_0 \\ -\hat{h}_0 - 2g\rho_0 & 0 \end{pmatrix} \begin{pmatrix} u \\ v \end{pmatrix}, \qquad \hat{h}_0 = -\tfrac{\hbar^2}{2m}\nabla^2 + V(\mathbf{r}), \tag{7}$$

which is the Bogoliubov–de Gennes (BdG) equation. In momentum space (with $V = 0$) the eigenvalues are:

$$E_k = \hbar\omega_k = \sqrt{\xi_k(\xi_k + 2g\rho_0)}, \qquad \xi_k = \frac{\hbar^2 k^2}{2m}. \tag{8}$$

The acoustic (phonon) branch $E_k \approx \hbar c_s k$ for $k\xi \ll 1$ and the free-particle branch $E_k \approx \xi_k$ for $k\xi \gg 1$, where $c_s = \sqrt{g\rho_0/m}$ and $\xi = \hbar/(mc_s\sqrt{2})$ is the healing length.

2.2 Bogoliubov transformation

The BdG system is diagonalised by the Bogoliubov transformation

$$\delta\psi_k = u_k\,\alpha_k + v_k\,\alpha^\dagger_{-k}, \qquad u_k^2 - v_k^2 = 1, \qquad u_k, v_k = \frac{1}{\sqrt{2}}\left(\sqrt{\frac{\xi_k + g\rho_0}{E_k}} \pm \sqrt{\frac{\xi_k + g\rho_0 - E_k}{E_k}}\right)^{1/2}, \tag{9}$$

yielding quasiparticle modes α_k (created/annihilated) with dispersion E_k. Residual cubic and quartic terms in $|\delta\psi|^3$ and $|\delta\psi|^4$ constitute the interaction vertices (Section 3.2).

3 Feynman Rules

3.1 Propagators

Rule P1 — Free (bare) quasiparticle propagator. For a coherence field excitation with momentum $\mathbf{k}$ and frequency ω:

$$G_0(\mathbf{k},\omega) = \frac{\hbar}{\hbar\omega - \dfrac{\hbar^2 k^2}{2m} - V_k + i\varepsilon}. \tag{10}$$

Represents a single-particle excitation of the field; pole at the free dispersion $\omega = \hbar k^2/(2m) + V_k/\hbar$.

Rule P2 — Dressed Bogoliubov propagator. After condensate factorisation, the full quasiparticle propagator is

$$G_B(\mathbf{k},\omega) = \frac{\hbar(\hbar\omega + \xi_k + g\rho_0)}{(\hbar\omega)^2 - E_k^2 + i\varepsilon}, \tag{11}$$

with E_k from (8). The anomalous (off-diagonal Nambu) component is $F(\mathbf{k},\omega) = -\hbar g\rho_0/[(\hbar\omega)^2 - E_k^2 + i\varepsilon]$.

Rule P3 — Phonon propagator. The acoustic Goldstone mode (density wave / sound wave):

$$D(\mathbf{k},\omega) = \frac{-\hbar^2/m}{(\hbar\omega)^2 - E_k^2 + i\varepsilon} \xrightarrow{k\xi\ll 1} \frac{-1/(\rho_0 m)}{\omega^2 - c_s^2 k^2 + i\varepsilon}. \tag{12}$$

Massless ($m_{\mathrm{ph}} = 0$); pole at the acoustic dispersion $\omega = c_s k$. In real space: $D(\mathbf{r},t) \sim \ln(r/\xi)/r$ at $t = 0$ (2D static limit).

Rule P4 — Vortex/soliton worldline propagator. A topological soliton of classical action S_{sol} and bare mass M_{sol} propagates as

$$\Delta_{\mathrm{sol}}(\mathbf{p},E) = \frac{1}{E - \mathbf{p}^2/(2M_{\mathrm{sol}}) + i\varepsilon}\, e^{-S_{\mathrm{sol}}/\hbar}, \tag{13}$$

where $e^{-S_{\mathrm{sol}}/\hbar}$ is the semiclassical weight. For a vortex: $M_v = \pi\hbar^2\rho_0/(g)\cdot\ln(R/\xi)$ (logarithmically UV divergent; cut off at the domain size R). For a bright soliton: $M_s = 2\hbar^2\rho_0/(g\xi_s)$ where $\xi_s = L_s$ is the soliton width.

Figure 1 shows the diagrammatic notation for all four propagator types.

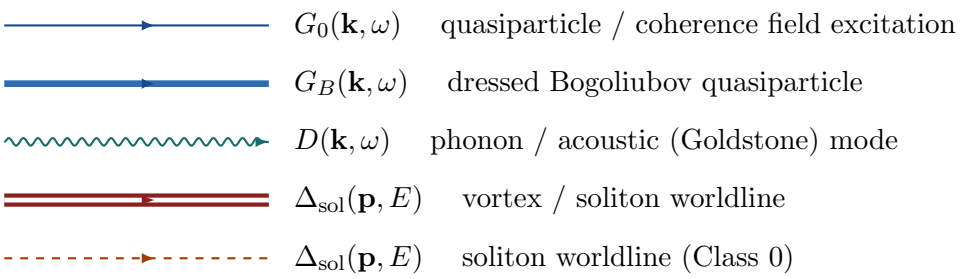

Figure 1: Propagator notation. Thin solid arrow: bare quasiparticle (P1). Thick solid arrow: dressed Bogoliubov quasiparticle (P2). Wavy arrow: phonon / acoustic mode (P3). Double solid arrow: vortex worldline (P4). Dashed arrow: soliton worldline (P4, Class 0 variant).

3.2 Vertices

Rule V1 — Contact four-point vertex. From the $-\frac{g}{2}|\psi|^4$ term in (5). Each vertex contributes a factor $-ig/\hbar$, along with a delta function enforcing energy–momentum conservation:

$$\text{Vertex factor:} \quad -\frac{ig}{\hbar}\,(2\pi)^3\,\delta^{(2)}\Big(\sum_i \mathbf{k}_i\Big)\,\delta\Big(\sum_i \omega_i\Big). \tag{14}$$

This vertex connects four field lines; in the Bogoliubov basis it decomposes into a sum of 2-quasiparticle and 4-quasiparticle terms.

Rule V2 — Condensate insertion (three-point) vertex. From the cross-term $-g\rho_0|\delta\psi|^2 - \frac{g\rho_0}{2}(\delta\psi^2 + \delta\psi^{*2})$ after Bogoliubov expansion. Two quasiparticle lines and one condensate "leg" (carrying the background density ρ_0):

$$\text{Vertex factor:} \quad -2ig\rho_0/\hbar. \tag{15}$$

Responsible for the anomalous pairing F and the generation of Bogoliubov coherence factors u_k, v_k.

Rule V3 — Vortex–phonon coupling vertex. A vortex of winding n moving with velocity $\mathbf{v}$ couples to a phonon of momentum $\mathbf{k}$ via the Magnus term in the action:

$$\Gamma_{vp}(\mathbf{k}, \mathbf{v}) = n\,\frac{\hbar}{m}\sqrt{\frac{\xi_k}{2E_k\rho_0}}\,\big(\hat{\mathbf{z}} \times \mathbf{k}\big)\cdot\hat{\mathbf{v}}, \tag{16}$$

where $\hat{\mathbf{z}}$ is the out-of-plane unit vector. This is the CFT analogue of the electron–photon vertex $-ie\gamma^\mu$. The coupling is proportional to n ("charge") and to $k^{1/2}$ (soft phonon behaviour analogous to the soft-photon limit in QED).

Rule V4 — External potential vertex. Coupling to an external field $V(\mathbf{r})$:

$$\text{Vertex factor:} \quad -iV(\mathbf{r})/\hbar. \tag{17}$$

For the Coulomb potential: $V(\mathbf{r}) = -\lambda_C/r$. For the harmonic trap: $V(\mathbf{r}) = \frac{1}{2}m\omega_0^2 r^2$.

Figure 2 catalogues the four vertex types diagrammatically.

3.3 Additional rules

1. **Loop integration:** Each closed loop contributes a factor $i\hbar\int d^2k\,d\omega/(2\pi)^3$.
2. **Symmetry factor:** Divide by the symmetry factor of each diagram (number of ways to relabel internal lines leaving the graph unchanged).
3. **Conservation at each vertex:** $\sum_i \mathbf{k}_i = 0$, $\sum_i \omega_i = 0$ (energy–momentum); winding number is conserved modulo pair creation/annihilation.

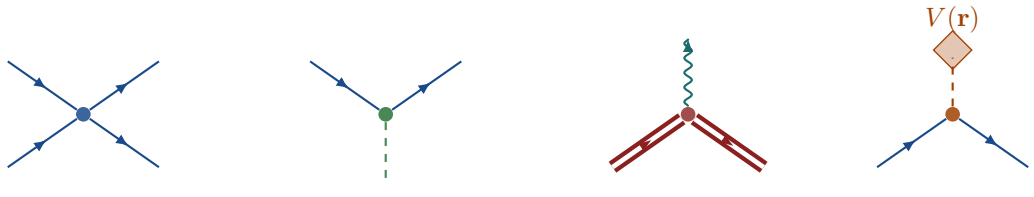

Figure 2: Vertex catalog. V1: Contact four-point vertex from $|\psi|^4$ (coupling $-ig/\hbar$). **V2:** Condensate insertion (three-point; dashed leg = $\sqrt{\rho_0}$ factor). **V3:** Vortex–phonon coupling from the Magnus term (winding n vortex emitting/absorbing an acoustic phonon). **V4:** External potential (harmonic trap or Coulomb).

4. **External lines:** Incoming quasiparticle: $G_0^{1/2}(\mathbf{k})$; outgoing quasiparticle: $G_0^{1/2*}(\mathbf{k})$; incoming/outgoing phonon: $[2E_k\rho_0/(m\xi_k)]^{1/2}$ (Bogoliubov coherence factor, normalising the phonon wavefunction).
5. **Winding-number conservation:** At any diagram, the total topological charge $\sum n_i$ of external lines is conserved. New vortex pairs ($n=+1$, $n=-1$ pair) may be produced internally at cost proportional to the vortex core energy $E_{\text{core}} = \pi\hbar^2\rho_0/(m)\ln(R/\xi)$.

4 Soliton Worldline Extension

For topological solitons (vortices, dark solitons) the path integral is dominated by the classical soliton saddle point. The effective action is decomposed as $S[\psi] = S_{\text{sol}}[\mathbf{r}_s(t)] + S_{\text{fluct}}[\delta\psi\,|\,\mathbf{r}_s]$, where $\mathbf{r}_s(t)$ is the collective coordinate (soliton position) and $\delta\psi$ are quantum/thermal fluctuations around the soliton background.

Integrating out $\delta\psi$ to one-loop gives the soliton effective action:

$$S_{\text{eff}}[\mathbf{r}_s] = \int dt \Big[\underbrace{\frac{1}{2}M_s\dot{\mathbf{r}}_s^2}_{\text{kinetic}} - \underbrace{E_{\text{sol}}}_{\text{rest energy}} + \underbrace{\hbar\,\Phi_B(\mathbf{r}_s)\dot{\mathbf{r}}_s}_{\text{Berry/Magnus}} + \underbrace{V_{\text{int}}(\mathbf{r}_1,\mathbf{r}_2)}_{\text{soliton–soliton}} \Big], \tag{18}$$

where Φ_B is the Berry phase generated by the background condensate. For a vortex at $\mathbf{r}_v$, the Berry term evaluates to $\Phi_B = \pi\hbar\rho_0\,\hat{\mathbf{z}}\times\mathbf{r}_v$, which is the Magnus force term: $\mathbf{F}_{\text{Magnus}} = \nabla\times(n\pi\hbar\rho_0\hat{\mathbf{z}}) = n\pi\hbar\rho_0\,\dot{\mathbf{r}}_v\times\hat{\mathbf{z}}$.

The soliton–soliton interaction potential V_{int} arises from the one-phonon-exchange Feynman diagram:

$$V_{\text{int}}(\mathbf{r}_1,\mathbf{r}_2) = \int \frac{d^2k}{(2\pi)^2}\,|\Gamma_{vp}(\mathbf{k})|^2\,D(\mathbf{k},\omega{=}0)\,e^{i\mathbf{k}\cdot(\mathbf{r}_1-\mathbf{r}_2)}. \tag{19}$$

Substituting (16) and (12) and integrating:

$$V_{\text{int}}(\mathbf{r}) = -\frac{n_1n_2\,\hbar^2\rho_0}{m}\ln\frac{r}{\xi} + \text{const} \qquad (n_1n_2 = \pm 1). \tag{20}$$

The sign n_1n_2 determines attraction ($-$, opposite winding) vs. repulsion ($+$, same winding) — the Magnus force law of CFT.

5 IX1: Vortex–Antivortex Annihilation

IX1 — Vortex–Antivortex Annihilation ($e^+e^- \to \gamma\gamma$ analogue)

Initial state: $|n{=}+1,\, \mathbf{p}_1\rangle \otimes |n{=}-1,\, \mathbf{p}_2\rangle$
Final state: $|\mathbf{k}_1\rangle_{\rm ph} \otimes |\mathbf{k}_2\rangle_{\rm ph}$ (two phonons)
Conservation: $n_1 + n_2 = 0$; $\mathbf{p}_1 + \mathbf{p}_2 = \mathbf{k}_1 + \mathbf{k}_2$; $E_1 + E_2 = \hbar\omega_1 + \hbar\omega_2$

5.1 Phase 0: pre-annihilation t-channel exchange

Before the cores meet, the two vortices interact by exchanging virtual phonons. This is the *t-channel* diagram (Figure 3, left), with amplitude

$$i\mathcal{M}^{(t)} = \left[\Gamma_{vp}(\mathbf{q}, \mathbf{v}_1)\right]^* \cdot iD(\mathbf{q}, 0) \cdot \Gamma_{vp}(\mathbf{q}, \mathbf{v}_2), \tag{21}$$

where $\mathbf{q} = \mathbf{p}_1 - \mathbf{p}_1'$ is the phonon momentum transfer. Summing over all $\mathbf{q}$ and Fourier-transforming recovers $V_{\rm int} \propto -\ln r$ (attractive for $n_1 n_2 = -1$).

5.2 Phase 1: annihilation tree diagram

When the vortex and antivortex cores overlap (separation $r \lesssim \xi$), the topological structure dissolves at a single *s-channel* contact vertex V1 emitting two phonons (Figure 3, right). The tree-level amplitude is

$$i\mathcal{M}^{(s)}_{\rm IX1} = \left(-\frac{ig}{\hbar}\right) \cdot \left[\Delta_v(\mathbf{p}_1)\right]^{1/2} \cdot \left[\Delta_{\bar v}(\mathbf{p}_2)\right]^{1/2} \cdot \left[D(\mathbf{k}_1)\right]^{1/2} \cdot \left[D(\mathbf{k}_2)\right]^{1/2}, \tag{22}$$

times the vortex–phonon form factor $\mathcal{F}(n_1, n_2; \mathbf{k}_1, \mathbf{k}_2)$ which enforces $n_1 + n_2 = 0$. The rate (analogue of a cross-section) is:

$$\Gamma_{\rm ann} \propto g^2\, \rho_0^2\, \left|\mathcal{F}\right|^2 \delta^{(2)}(\mathbf{p}_1 + \mathbf{p}_2 - \mathbf{k}_1 - \mathbf{k}_2)\, \delta(\omega_1 + \omega_2 - E_1/\hbar - E_2/\hbar). \tag{23}$$

The norm loss observed in the GPE simulation ($\approx 30\%$ over $T \in [0, 4]$) is the integrated flux of outgoing phonon radiation.

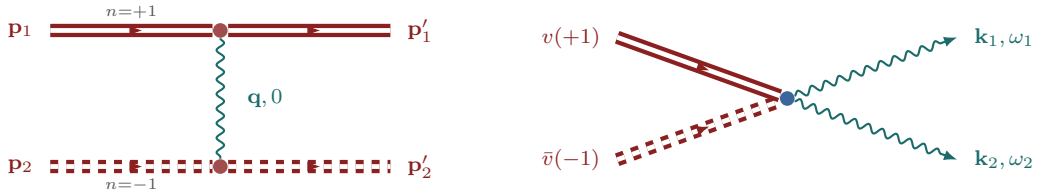

(a) Pre-annihilation t-channel phonon exchange

(b) Annihilation tree s-channel, vertex V1

Figure 3: IX1 Feynman diagrams. (a) Pre-annihilation t-channel virtual phonon exchange mediating the Magnus attraction ($n_1 n_2 = -1$, attractive). **(b)** Tree-level s-channel annihilation at the contact vertex V1: the two vortex worldlines terminate and two real phonons are emitted. Double arrows: vortex ($n = +1$, solid) and antivortex ($n = -1$, dashed double) worldlines. Wavy arrows: outgoing phonons.

Feynman series structure. The full amplitude is $\mathcal{M}_{\text{IX1}} = \mathcal{M}^{(s)} + \mathcal{M}^{(t)} + \mathcal{M}^{(s,\text{1-loop})} + \cdots$. The dominant term at large separation is the t-channel exchange (generates the attractive logarithmic potential driving approach); the dominant term at contact is the s-channel tree diagram (the actual annihilation). Loops contribute α_{CFT}^n corrections at each order. SM analogue: $e^+e^- \to \gamma\gamma$ (s-channel) via virtual photon (t-channel Coulomb approach precedes the annihilation event).

6 IX2: Same-Charge Vortex Repulsion

IX2 — Same-Charge Vortex Repulsion (Coulomb analogue)

Initial state: $|n{=}{+}1,\, \mathbf{p}_1\rangle \otimes |n{=}{+}1,\, \mathbf{p}_2\rangle$
Final state: $|n{=}{+}1,\, \mathbf{p}_3\rangle \otimes |n{=}{+}1,\, \mathbf{p}_4\rangle$
Conservation: $n_1 + n_2 = n_3 + n_4 = +2$; $\mathbf{p}_1 + \mathbf{p}_2 = \mathbf{p}_3 + \mathbf{p}_4$

6.1 One-phonon exchange (Born approximation)

The leading-order scattering diagram is the *t-channel one-phonon exchange* (Figure 4). Each vortex emits/absorbs one phonon at a V3 vertex; the phonon propagates as a virtual (off-shell) internal line:

$$i\mathcal{M}_{\text{IX2}}^{(\text{1-ph})} = \left[\Gamma_{vp}(\mathbf{q})\right]^2 \cdot iD(\mathbf{q}, \omega{=}0), \quad \mathbf{q} = \mathbf{p}_3 - \mathbf{p}_1. \tag{24}$$

Substituting the vertex (16) and propagator (12):

$$\mathcal{M}_{\text{IX2}}^{(\text{1-ph})} \propto \frac{n_1 n_2\, \hbar^2 \rho_0/m}{q^2 + \xi^{-2}}, \tag{25}$$

which Fourier-transforms to the Yukawa potential at range ξ. In the long-range limit $q\xi \ll 1$:

$$V_{\text{rep}}(r) = +\frac{n_1 n_2\, \hbar^2 \rho_0}{m} \ln \frac{r}{\xi} \qquad (\text{repulsive for } n_1 n_2 = +1), \tag{26}$$

recovering equation (20) with $n_1 n_2 = +1$.

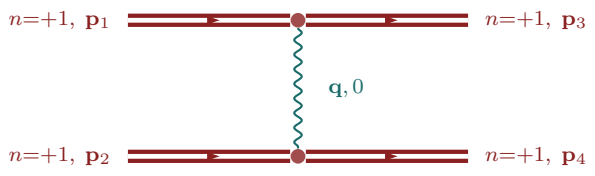

One-phonon exchange (Born approx.)

Figure 4: IX2 Feynman diagram. t-channel one-phonon exchange between two same-sign ($n_1 = n_2 = +1$) vortices. The virtual phonon (wavy internal line) carries momentum transfer $\mathbf{q}$. The winding number $n_1 n_2 = +1 > 0$ makes the potential repulsive, in direct analogy with Coulomb repulsion between like charges. Higher-order diagrams (two-phonon exchange, etc.) add $O(\alpha_{\text{CFT}}^2)$ corrections.

6.2 Higher-order ladder and comparison with Abrikosov lattice

At higher orders, repeated phonon exchange produces a ladder diagram series

$$V_{\text{eff}}(r) = V^{(1)} + V^{(2)} + \cdots = \frac{n^2\hbar^2\rho_0}{m} \ln\frac{r}{\xi}\Big[1 + \alpha_{\text{CFT}}\, f_1(r/\xi) + \cdots\Big], \tag{27}$$

where f_1 is a dimensionless function. For N same-sign vortices, the minimum energy configuration has them arranged in a triangular (Abrikosov) lattice with spacing $a = (4\pi/(\sqrt{3}N))^{1/2}L$. This crystalline ground state is the exact analogue of type-II superconductor Abrikosov lattice and of Wigner crystal formation in 2D electron gases.

Feynman series structure. Unlike IX1, there is no s-channel process: the winding number conservation ($\sum n_i = +2$ conserved) prevents annihilation. All diagrams are t-channel, and the infinite ladder sums to give an exact $\ln r$ potential. SM analogue: Coulomb repulsion between two electrons, mediated by virtual photon exchange. The phonon plays the role of the photon; the Magnus phase replaces the electromagnetic phase.

7 IX3: Bright Soliton Head-on Collision

IX3 — Bright Soliton Head-on Collision (integrable elastic scattering)

Initial state: $|s_1,\, k\rangle \otimes |s_2,\, -k\rangle$ (two solitons approaching)
Final state: $|s_1,\, k'\rangle \otimes |s_2,\, -k'\rangle$ (two solitons departing, with phase shift)
Conservation: winding $n = 0$ both sides; $|k| = |k'|$ (elastic); E conserved

7.1 Tree-level (Born) amplitude

The leading-order soliton–soliton interaction vertex is the cross-density contact term:

$$S_{\text{ss}} = -g \int dt\, d^2r\; |\psi_{s_1}|^2 |\psi_{s_2}|^2, \tag{28}$$

giving a tree-level scattering amplitude (Figure 5a):

$$i\mathcal{M}^{(\text{tree})}_{\text{IX3}} = (-ig) \int d^2r\; |\psi^*_{s_1}(\mathbf{r})|^2\, |\psi^*_{s_2}(\mathbf{r})|^2. \tag{29}$$

For two sech profiles separated by d, this integral is exponentially small for $d \gg L_s$ and $O(1)$ at contact. The resulting Born phase shift:

$$\delta_{\text{Born}}(k) = -\frac{m\, g\, \rho_s}{2\hbar^2 k} \int_{-\infty}^{\infty} |\psi^*_s(x)|^2\, dx = -\frac{mg\rho_s L_s}{\hbar^2 k}, \tag{30}$$

where ρ_s is the peak soliton density.

7.2 Ladder resummation and exact S-matrix

The full Feynman series for soliton–soliton scattering in 1D consists of *ladder diagrams* (Figure 5b): n-th order has n rungs (phonon exchanges) connecting the two soliton worldlines. For the 1D nonlinear

Schrödinger equation (NLSE), the model is integrable (Zakharov–Shabat / inverse scattering transform); the Yang–Baxter equation holds and the ladder series can be summed exactly. The exact two-soliton S-matrix is:

$$S_{12}(k) = e^{2i\delta(k)}, \qquad \delta(k) = \arctan\left(\frac{2kL_s}{k^2L_s^2 - 1}\right), \tag{31}$$

where k is the relative momentum and L_s is the soliton width. The modulus $|S_{12}| = 1$ confirms elastic scattering. No topology is exchanged: the soliton number (2 in, 2 out) and winding number (both zero) are separately conserved.

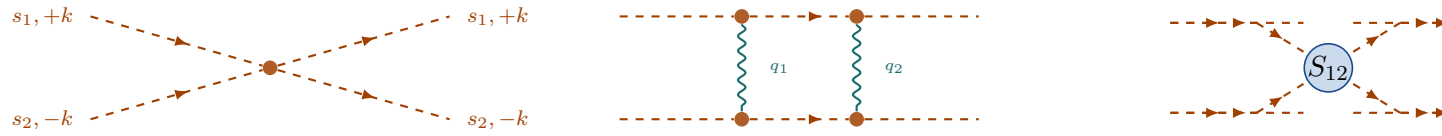

(a) Tree level ($n = 1$) (b) Two-rung ladder ($n = 2$) (c) All-orders resumm $S_{12} = e^{2i\delta(k)}$

Figure 5: IX3 Feynman diagram series. (a) Tree-level (Born) contact vertex; gives phase shift δ_{Born}. **(b)** Two-rung ladder: two soliton worldlines (dashed) connected by two virtual phonon rungs (wavy); next-to-leading order. **(c)** All-orders resummed S-matrix blob $S_{12} = e^{2i\delta(k)}$; the infinite ladder is summable exactly by the Yang–Baxter equation of the integrable 1D NLSE.

Feynman series structure. The series is all-t-channel ladder diagrams with $n = 1, 2, 3, \ldots$ rungs. Each rung is a virtual phonon exchange (P3) connecting the two soliton worldlines (P4) at V1 vertices. The infinite sum is geometrically convergent (integrable NLSE; the ladder is the exact Bethe Ansatz series) and yields the exact phase shift. The CFT analogue is the Manakov *pp*-scattering series.

8 IX4: Dark Soliton × Vortex Composite

IX4 — Dark Soliton × Vortex Composite (flux tube × monopole analogue)

Initial state: $|\text{ds}\rangle \otimes |n{=}{+}1\rangle$ (dark soliton stripe × vortex)
Intermediate / final: $\mathbb{Z}_2$-broken composite + secondary vortex pairs
Key effect: explicit $\mathbb{Z}_2$ symmetry breaking by the vortex phase

8.1 Mixed-topology vertex

The dark soliton (D2) carries a π phase kink: $\psi_{\text{ds}}(x) = \sqrt{\rho_\infty}\tanh\big(x/\sqrt{2}\xi\big)$; the phase jumps by π at $x = 0$. The vortex (B1) carries a 2π winding around its core. The product state has an interaction energy

$$V_{\text{mix}} = \frac{\hbar^2}{2m}\int d^2r\,(\nabla\theta_{\text{ds}})\cdot(\nabla\theta_v) = \frac{\hbar^2}{2m}\int d^2r\,\nabla\cdot(\theta_{\text{ds}}\,\nabla\theta_v), \tag{32}$$

which is the *mixed-topology vertex* (Figure 6). Using $\nabla^2\theta_v = 2\pi n\,\delta^{(2)}(\mathbf{r}-\mathbf{r}_v)$ for a vortex at $\mathbf{r}_v$ and $\theta_{\rm ds}(x=0^+) - \theta_{\rm ds}(x=0^-) = \pi$:

$$V_{\rm mix}(\mathbf{r}_v) = \frac{\pi n\hbar^2}{2m}\,\theta_{\rm ds}(\mathbf{r}_v) = \begin{cases} 0 & (x_v < 0) \\ \frac{\pi^2 n\hbar^2}{4m} & (x_v = 0) \\ \frac{\pi^2 n\hbar^2}{2m} & (x_v > 0) \end{cases}. \tag{33}$$

This potential is step-like at the soliton stripe: the vortex is *reflected* or *transmitted* depending on the relative orientation, and the stripe explicitly breaks the $\mathbb{Z}_2$ symmetry $x \to -x$ of the dark soliton (Figure 6).

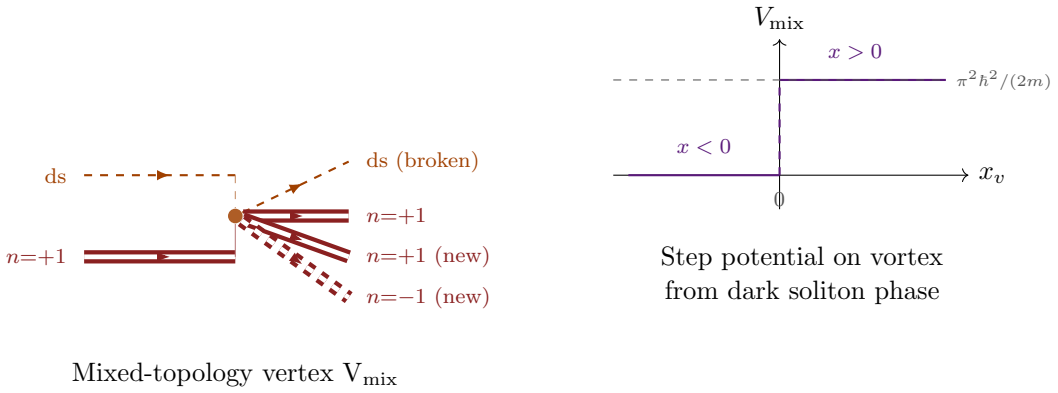

Figure 6: IX4 mixed-topology vertex. Left: Dark soliton (dashed arrow) and vortex (double arrow) enter the mixed-topology vertex $V_{\rm mix}$; the outgoing state has a symmetry-broken soliton and can nucleate a secondary vortex–antivortex pair. **Right:** Effective step potential (33) experienced by the vortex as a function of its position x_v relative to the dark soliton stripe at $x = 0$. The discontinuity explicitly breaks the $\mathbb{Z}_2$ symmetry $x_v \to -x_v$ of the pure dark soliton.

Feynman series structure. The leading term is the mixed-topology vertex $V_{\rm mix}$, which is not present in either the pure vortex or pure dark soliton theories alone. It arises from the cross-gradient coupling in the kinetic energy. Higher-order diagrams involve repeated phonon exchange between the composite soliton and the vortex, plus loop corrections from secondary vortex-pair creation. SM analogue: the flux-tube–monopole composite (Abrikosov vortex threading a magnetic monopole in the Georgi–Glashow model), where the mixed-topology vertex is the direct coupling between the gauge flux and the magnetic charge.

9 IX5: Breathing Mode × Soliton Impurity

IX5 — Breathing Mode × Soliton Impurity (phonon–impurity Feshbach analogue)

Initial state: $|F_1, \omega_B\rangle \otimes |\text{sol}\rangle$ (breathing condensate + soliton defect)
Observable: shifted breathing frequency $\omega_B' \neq \omega_B$; amplitude modulation of $\langle r^2\rangle(t)$
Mechanism: phonon self-energy insertion from soliton scattering

9.1 Unperturbed breathing mode

The Thomas–Fermi condensate in a harmonic trap $V(r) = \frac{1}{2}m\omega_0^2 r^2$ has a monopole (breathing) mode at the Kohn frequency:

$$\omega_B = 2\omega_0\sqrt{\kappa}, \qquad \kappa = \lambda_V m\omega_0^2/(g\rho_{\rm TF}), \tag{34}$$

where $\rho_{\rm TF}$ is the central Thomas–Fermi density and λ_V is the confinement strength parameter. The breathing mode is a coherent superposition of phonons with wavevectors $k_B = \omega_B/c_s$; its propagator is:

$$G_{\rm br}(\omega) = \frac{Z_B}{\omega - \omega_B + i\varepsilon}, \qquad Z_B = \frac{2\omega_B}{g\rho_{\rm TF}}. \tag{35}$$

9.2 Self-energy from soliton impurity

The soliton at position $\mathbf{r}_s$ is a localised density notch $\rho_{\rm sol}(\mathbf{r}) = \rho_0[1 - \operatorname{sech}^2(|\mathbf{r} - \mathbf{r}_s|/L_s)]$. A breathing-mode phonon scatters off this notch via the contact vertex V1, producing the one-loop self-energy diagram (Figure 7):

$$-i\Sigma(\omega) = (-ig)^2 \int \frac{d^2k\, d\nu}{(2\pi)^3}\, G_{\rm br}(\omega - \nu)\, |T_{\rm sol}(k,\nu)|^2, \tag{36}$$

where $T_{\rm sol}(\mathbf{k},\nu)$ is the soliton T-matrix (single-soliton scattering amplitude for an incident phonon of wavevector k and frequency ν):

$$T_{\rm sol}(k) = -\frac{gM_s/\hbar}{\xi_k + gM_s/\hbar + i\varepsilon}, \qquad M_s = \frac{2\hbar^2\rho_0}{gL_s}. \tag{37}$$

The real part of $\Sigma(\omega)$ at $\omega = \omega_B$ gives the frequency shift:

$$\delta\omega_B = \frac{\operatorname{Re}\Sigma(\omega_B)}{2\omega_B} \approx -\frac{M_s}{2M_{\rm cond}}\,\omega_B \qquad \big(M_s \ll M_{\rm cond}\big), \tag{38}$$

where $M_{\rm cond} = \int \rho_{\rm TF}\, d^2r$ is the total condensate norm. This is the CFT analogue of the phonon self-energy renormalization from an impurity in a BEC: the soliton mass-loads the condensate, lowering $\omega_B' = \omega_B + \delta\omega_B$.

The imaginary part $\operatorname{Im}\Sigma(\omega_B)$ gives a finite linewidth (damping rate):

$$\Gamma_B = \frac{\operatorname{Im}\Sigma(\omega_B)}{\omega_B} \propto g^2 M_s \rho_0(k_B)\, \omega_B^{-1}, \tag{39}$$

which manifests as the amplitude modulation seen in $\langle r^2\rangle(t)$.

Feynman series structure. This is a *self-energy insertion* (one-particle irreducible diagram). The bare propagator $G_{\rm br}(\omega)$ is dressed by the soliton-scattering loop to give $G'_{\rm br}(\omega) = 1/(\omega - \omega_B - \Sigma(\omega))$. The full Dyson series is the geometric series of all self-energy insertions. At lowest order (38): mass loading from the soliton decreases ω_B. Higher loops ($\alpha^2_{\rm CFT}$ and beyond) modify the line shape. SM analogue: phonon–impurity coupling in condensed matter (Feshbach resonance); the breathing frequency shift corresponds to mass renormalization of the composite boson.

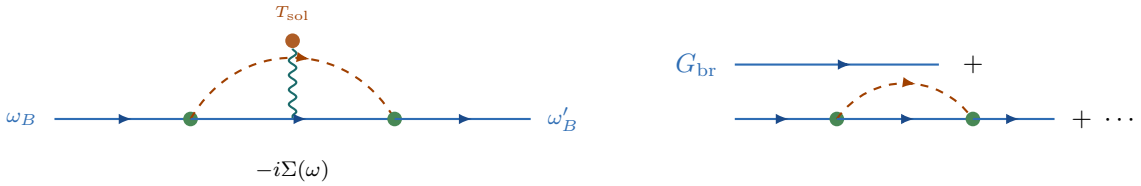

One-loop self-energy insertion
$\omega'_B = \omega_B + \delta\omega_B$

Dyson: $G'_{\rm br} = G_{\rm br}/(1 - \Sigma G_{\rm br})$

Figure 7: IX5 self-energy diagrams. Left: One-loop self-energy $-i\Sigma(\omega)$: the breathing-mode phonon (thick blue arrow) emits and reabsorbs a virtual soliton (dashed loop) via the soliton T-matrix vertex $T_{\rm sol}$ (orange dot), dressed by the contact vertices (green dots). The virtual phonon (wavy internal line) connects the soliton loop to the main line. **Right:** Dyson equation in diagrammatic form: the full propagator $G'_{\rm br}$ is the geometric series of self-energy insertions. The dressed pole gives the shifted frequency $\omega'_B = \omega_B + \delta\omega_B$ and finite linewidth Γ_B.

10 Summary: Interaction Taxonomy and Loop-Order Counting

10.1 Comparison table

ID	Process	Leading diagram	Vertex(es)	Series type	SM analogue
IX1	$v_+ + v_- \to \gamma + \gamma$	s-channel contact; t-channel pre-collision phonon exchange	V1, V3	Tree (annihilation) + Born series (approach)	$e^+e^- \to \gamma\gamma$
IX2	$v_+ + v_+ \to v_+ + v_+$	t-channel one-phonon exchange	V3 × 2	All-order ladder $\to \ln r$ potential	Coulomb e^-e^- repulsion
IX3	$s + s \to s + s$	t-channel contact; infinite ladder	V1 × n	Integrable ladder (Yang–Baxter); exact $e^{2i\delta}$	pp elastic scattering / Manakov solitons
IX4	$\mathrm{ds} + v \to$ composite	Mixed-topology vertex $V_{\rm mix}$	$V_{\rm mix}$ (kinetic cross-gradient)	Tree + pair-creation loop	Flux tube × monopole
IX5	$F_1 + \mathrm{sol} \to F_1'$	One-loop self-energy $\Sigma(\omega)$	V1, $T_{\rm sol}$	Dyson resummation $\to$ dressed propagator	Phonon–impurity (Feshbach)

10.2 Loop-order counting and convergence

For a diagram with V vertices, I internal lines, and L loops:

$$L = I - V + 1 \quad \text{(connected diagram)}, \qquad \text{power of } \alpha_{\text{CFT}} : \ \alpha_{\text{CFT}}^{V}. \tag{40}$$

Diagram	V	I	L	**Order**
IX1 tree (s-ch.)	1	0	0	α^1
IX2 one-phonon exchange	2	1	0	α^2
IX3 n-rung ladder	$2n$	$n{+}1$	0	α^{2n}
IX4 tree	1	0	0	α^1 (effective)
IX5 one-loop self-energy	2	2	1	α^2
IX5 two-loop	4	5	2	α^4

Note: since $\alpha_{\text{CFT}} \sim 1$ in CFT units, the loop expansion is not small. The exact results for IX2 and IX3 are resummed series (entire ladder → closed-form potential / S-matrix). The IX5 Dyson series sums all self-energy insertions to give the dressed propagator with shifted pole.

10.3 Winding-number selection rules

ID	**Process**	Δn_{total}
IX1	$n{=}+1$ vortex + $n{=}-1$ antivortex → phonons ($n{=}0$)	$+1+(-1)=0$
IX2	$n{=}+1$ vortex + $n{=}+1$ vortex → $+1+1$ (elastic)	$+2=+2$
IX3	soliton($n{=}0$) + soliton($n{=}0$) → 2 solitons	$0=0$
IX4	dark soliton($n{=}0$) + vortex($n{=}+1$) → composite + pair	$+1=+1$ (vortex pair: $+1{-}1=0$)
IX5	breathing($n{=}0$) + soliton($n{=}0$) → shifted breathing	$0=0$

In every case total winding is conserved, just as total electric charge is conserved in QED. The topological conservation law $\Delta n = 0$ is protected by $\pi_1(S^1) = \mathbb{Z}$ and cannot be violated at any finite order in perturbation theory.

10.4 The phonon as the CFT gauge boson

The structural analogy between CFT and QED can now be made precise:

QED	**CFT (2D)**
Photon propagator $D_{\mu\nu}(k)$	Phonon propagator $D(k,\omega)$ (12)
Electron–photon vertex $-ie\gamma^\mu$	Vortex–phonon vertex $\Gamma_{vp}(\mathbf{k},\mathbf{v})$ (16)
Electric charge $q=-e$	Topological charge $n=\pm1,\pm2,\ldots$
Coulomb potential $V(r)=e^2/(4\pi r)$	Magnus potential $V(r)=n^2\ln(r/\xi)$
Fine structure constant $\alpha\approx 1/137$	CFT coupling $\alpha_{\mathrm{CFT}}=mg/\hbar^2\approx 1$
$e^+e^-\to\gamma\gamma$ (annihilation)	$v_+v_-\to$ phonons (IX1)
Compton scattering $e\gamma\to e\gamma$	Vortex–phonon scattering
Pair production $\gamma\to e^+e^-$	Phonon $\to$ vortex pair (pair creation)

The essential difference: in QED the gauge symmetry is local $U(1)$ and the photon is massless by a gauge principle; in CFT the phonon is massless as the Nambu–Goldstone mode of the spontaneously broken global $U(1)$ of the condensate. The masslessness is not protected by a gauge principle but by the Goldstone theorem.